Journal of Innovative Optical Health Sciences
Vol. 2, No. 4 (2009) 387–396

World Scientific
www.worldscientific.com

Fc-DIRECTED ANTIBODY CONJUGATION OF MAGNETIC NANOPARTICLES FOR ENHANCED MOLECULAR TARGETING

ROBABEH REZAEIPOOR†, RENU JOHN†, STEVEN G. ADIE†,
ERIC J. CHANEY†, MARINA MARJANOVIC†, AMY L. OLDENBURG†,
STEPHANIE A. RINNE† and STEPHEN A. BOPPART*,†,‡
†*Biophotonics Imaging Laboratory*
Beckman Institute for Advanced Science and Technology
University of Illinois at Urbana-Champaign, Urbana, IL, USA
‡*Departments of Electrical and Computer Engineering,*
Bioengineering, and Internal Medicine
University of Illinois at Urbana-Champaign
Urbana, IL, USA
**boppart@illinois.edu*

In this study, we report the fabrication of engineered iron oxide magnetic nanoparticles (MNPs) functionalized with anti-human epidermal growth factor receptor type 2 (*HER2*) antibody to target the tumor antigen *HER2*. The Fc-directed conjugation of antibodies to the MNPs aids their efficient immunospecific targeting through free Fab portions. The directional specificity of conjugation was verified on a macrophage cell line. Immunofluorescence studies on macrophages treated with functionalized MNPs and free anti-*HER2* antibody revealed that the antibody molecules bind to the MNPs predominantly through their Fc portion. Different cell lines with different *HER2* expression levels were used to test the specificity of our functionalized nanoprobe for molecular targeting applications. The results of cell line targeting demonstrate that these engineered MNPs are able to differentiate between cell lines with different levels of *HER2* expression.

Keywords: Nanoprobe; molecular imaging; cancer.

1. Introduction

Nanoparticles play an important role as imaging contrast agents in various biomedical imaging modalities including fluorescence microscopy,[1–4] positron emission tomography (PET),[5] single photon emission computed tomography (SPECT),[5,6] ultrasound imaging,[7] magnetic resonance imaging (MRI),[8,9] plasmon resonance scattering,[10] optical coherence tomography (OCT),[11,12] and magnetomotive OCT (MM-OCT).[13] With the recent developments in the synthesis and functionalization of nanoparticles, the field of nanomedicine holds a promising future with potential applications in the early diagnosis of disease,[14] site-specific drug delivery[15–18] and therapeutic applications utilizing hyperthermia.[19,20]

Various molecular imaging agents such as quantum dots,[2–4] gold nanoshells,[14] carbon nanotubes,[19] gold nanoparticles,[10] Gadolinium nanoparticles,[21] superparamagnetic iron oxide nanoparticles,[8,9,16]

polymeric nanoparticles[22] and microspheres,[12] have been reported in the literature as contrast agents for different imaging modalities. With the reported early successes in clinical oncology imaging, superparamagnetic iron oxide nanoparticles hold a very promising role as molecular nanoprobes for imaging and hyperthermia applications.[15–20] Iron oxide nanoparticles possess unique paramagnetic properties that result in strong T_2 and T_2^* contrast, making them ideal for MRI studies.[23] Due to their paramagnetic nature, iron oxide magnetic nanoparticles (MNPs) can be modulated by an external magnetic field, creating dynamic contrast in MM-OCT.[13] Several different synthetic and natural polymers including dextran and its derivatives,[24,25] polyethylene glycols (PEGs),[26,27] and polyvinylpyrolidone[27,28] have been employed to coat the surface of iron oxide MNPs to improve their dispersibility in aqueous media, biocompatibility and biodegradability for *in vivo* applications.

Functionalization for targeting specific molecular sites is yet another important and most desirable quality of the nanoprobes. The first generation of nanoparticle-based therapy aimed at the passive delivery of nanoparticles to specific sites like tumors, exploiting the enhanced permeability and retention (EPR) effect associated with the leaky vasculatures.[17] However, this enhanced permeability and retention is not a consistent feature of tumor vessels[15,29] and fast uptake of nanoparticles by the reticulo-endothelial system (RES) resulted in their rapid clearance from the circulation. Hence, relatively low concentration of nanoparticles at targeting sites was a major obstacle in using them for tumor imaging or therapy. Efficient ways to target malignant cells have been reported by conjugating the nanoparticles with antibodies targeted to specific markers or oncoproteins,[8,10,20,23] which are known to be overexpressed in the malignant cells. However, the conjugating procedures are challenging and depend on the nature of the coating of the nanoparticles and the conjugating ligand or proteins.[20,23] Commonly, the contrast agent is targeted to a specific receptor or antigen by using a specific antibody molecule or its Fab fragment (antigen-binding fragment). Most conjugation methods using a carbodiimide mediator target the primary amino-group present at the Fab fragment or active site of the antibody molecule. Using this conjugation method, the final product has a limited number of functional and active groups for efficient targeting.[30,31] To overcome this limitation, a conjugation method should be designed to target the Fc fragment (non-antigen binding fragment) of an antibody molecule through its carboxyl, hydroxyl, sulfhydryl or thiol groups.[32–37]

Among the various biomarkers, one of the most well-known targeted proteins is the human epidermal growth factor receptor 2 (*HER2*, also known as *c-erbB-2/neu*), which is a receptor protein overexpressed in about 30% of human invasive breast carcinomas.[10,18,34,36] This receptor is expressed at the membrane surfaces making it easier to target by the nanoparticle conjugates.

In this manuscript we demonstrate the advantage of Fc-directed conjugation of iron oxide MNPs in active targeting applications. We describe the fabrication of engineered iron oxide MNPs coated with dextran and functionalized with anti-*HER2* antibody to target *HER2* antigen in human breast carcinomas. The Fc-directed specificity of conjugation is verified on a macrophage cell line. Immunostaining of macrophages treated with functionalized MNPs and free anti-*HER2* antibodies showed that the antibody molecules bind to the MNPs predominantly through its Fc portion. Different cell lines with different *HER2* expression levels were used to test the specificity of our functionalized nanoprobe for molecular targeting applications. These Fc-directed MNPs can act as multimodal imaging agents with *in vitro* and *in vivo* applications in magnetomotive imaging, targeted drug delivery, and therapeutic applications.

2. Materials and Methods

2.1. *Preparation of targeted iron oxide MNPs*

Iron oxide-dextran nanoparticles (Fe-Dex-MNPs) were synthesized by the coprecipitation of ferrous and ferric salts in the presence of the polymer dextran in alkaline medium following standard protocols.[9,34,37–39] A mixed solution of ferrous and ferric ions in a molar ratio equal to 0.57 was prepared from 6.4% $FeCl_2 \cdot 4H_2O$ and 15.1% $FeCl_3 \cdot 6H_2O$ in deaerated, distilled water. An equal volume of a 20% (w/v) polymer solution in distilled water was then mixed with the iron solution and kept at a constant temperature of 60°C for 15 minutes under nitrogen purging to avoid oxidation. An approximately equal volume of 7.5% (v/v) aqueous ammonia solution was then added dropwise to the iron-polymer mixture to maintain the pH at 11.5 during heating at 60°C for 15 minutes, with

vigorous stirring. The unbound dextran was separated from MNPs by molecular sieve chromatography using a Sephadex G-300 column equilibrated with 0.01 M phosphate buffer at pH 7.4. After fractionation, the anthrone assay was used to determine the presence of any unbound dextran in the eluted fractions.[38]

Fc-directed conjugation of the antibody molecules is made possible through reductive amination coupling between the free amino groups in the Fc-region of the antibody and reactive aldehyde groups. To create reactive aldehyde groups on the MNP surfaces, oxidation of dextran is carried out under mild conditions. A volume of 0.25 ml of 25 mmol/L $NaIO_4$ (final concentration 5 mmol/L[40]) was used to oxidize 1 ml of Fe-Dex-MNPs. The reaction was kept away from light and oxygen, and was constantly stirred (150 r/min). Next, 0.2 ml of 2 mol/L ethylene glycol was added and stirred for another 30 minutes to terminate oxidation. Excess periodate was removed by dialyzing the suspension for 24 hours against 0.01 mol/L PBS at 4°C. A quantity of 10 to 25 μg/mg of rabbit polyclonal anti-HER2 antibody (c-erbB-2/neu, Thermo Fisher Scientific, Cat. #RB-103PABX) was added to the oxidized Fe-Dex-MNPs under dark conditions at 4°C for 8 h. This step was followed by reduction with 0.5 mol/L $NaBH_4$ for 30 minutes to stabilize the new configuration. Uncoupled antibody was separated from conjugated particles by gel filtration chromatography on a Sephacryl S 300 column. The final antibody/nanoparticle ratio (valence) was determined using a bicinchoninic acid (BCA) assay (Protein Quantitation Assay, Pierce, Rockford, IL, USA).

2.2. *Particle size determination using TEM*

MNPs in 20 to 40 μl aqueous (0.01 M phosphate buffer pH 7.4) suspensions were placed on glow-discharged (DPG-1 portable glow-discharge system, Denton Vacuum Inc., Moorestown NJ) 200-mesh carbon-stabilized Formvar-coated copper TEM grids (Cat. No. 01811, Ted Pella Inc., Redding CA), and the liquid was allowed to evaporate. Grids were then imaged using a transmission electron microscope (TEM) (Philips CM200, FEI Co., Hillsboro, OR) at 120 kV. Images were collected using a TVIPS 2k × 2k Peltier-cooled CCD camera (Tietz Video and Image Processing Systems GmbH, Gauting, Germany). The scale bar was automatically added by the TEM software.

2.3. *Cell culture*

Human umbilical vein endothelial cells (HUVEC) (Cambrex Bio Science Walkersville, Inc.) and rat mammary adenocarcinoma tumor (MAT) cells (13762 MAT BIII, ATCC) were used because they display little to moderate amounts of *HER2* expression, respectively. A human breast adenocarcinoma cell line (SKBR-3, ATCC) was used as a positive cell line for *HER2* overexpression. Mouse macrophages (MØ, ATCC) were used as a source of Fc receptor-expressing cells to test the free and bound Fc portions of the antibody molecules used for conjugation. A human breast primary ductal carcinoma cell line (CRL-2314, ATCC) was used as a cell line with minimal *HER2* expression.

The HUVEC cell line was grown using the EGM-2 BulletKit (CC-3162, Cambrex Bio Science Walkersville, Inc.). The MAT and SKBR-3 cell lines were grown in modified McCoy's 5a medium (ATCC), and macrophages and CRL-2314 cells were grown in DMEM and RPMI 1640 (complete growth medium with 10% fetal bovine serum, ATCC) respectively. All cell lines were cultured at 37°C in a humidified CO_2 incubator (5% CO_2 and 95% air). A 1% mixture of an antibiotic-antimycotic agent (Penicillin G, Streptomycin sulfate, and Amphotericin B, Sigma, A5955) was also added to all cell culture media, except the EGM-2 BulletKit.

2.4. *Specific antibodies*

Rabbit polyclonal anti-*HER2* antibody (c-erbB-2/*HER-2/neu* Ab-1 (21n) (Thermo Scientific, Cat. #RB-103-PABX) was used at a concentration of 1 mg/ml to construct the targeted MNPs. The c-erbB-2 antibody has a known reactivity to *HER2* for rat tumor models. For immunostaining after *in vitro* targeting, FITC-conjugated donkey anti-rabbit IgG (H + L) was used as a secondary antibody (Jackson ImmunoResearch Laboratories, Inc.).

2.5. *Cell line targeting*

Approximately 10^6 cells from each cell line were grown on sterile, round microscope cover slips (Fisher brand) in sterile Petri dishes with cell culture media. After 24 hours, the cover slips were

washed three times in sterile $1 \times$ PBS. Cells were fixed with ice-cold acetone for 15 minutes at 4°C and kept at −20°C until use. Cell monolayers were washed three times using $1 \times$ PBS, blocked with 10% normal donkey serum (in $1 \times$ PBS + 1% BSA) for 30 minutes at room temperature inside a humidity chamber, and washed three times for two minutes in washing buffer ($1 \times$ PBS + 0.1% Tween 20). Cover slips were then incubated with either targeting solution [anti-*HER2* antibody (100 μl of $100 \times$ diluted), Ab-Dex-MNPs (100 μl of 1 mg/ml solution), Dex-MNPs (100 μl of 1 mg/ml solution)] or just PBS buffer (100 μl), for 90 minutes at room temperature inside a humidity chamber. After incubation cover slips were washed three times for two minutes with washing buffer, and then incubated with secondary antibody (1:200 dilution) for 60 minutes inside the humidity chamber. After washing cover slips another three times for two minutes with washing buffer, they were mounted onto a microscope slide using a hard set mounting medium (H-1400, Vectashield, Vector Laboratories, Inc.). The samples were viewed with fluorescence microscopy (Axiovert 200, Carl Zeiss).

2.6. *Quantification of fluorescence signal*

All fluorescence images were acquired under the same microscope illumination, camera gain, and exposure settings. Cell line monolayers were confirmed in the field-of-view under brightfield illumination before fluorescence imaging. Analysis was performed in MatLab^{TM} on the raw 8-bit, $1{,}600 \times 1{,}200$ pixel images to quantify the detected fluorescence signals. Due to cell monolayers not being uniformly distributed over the cover slips, ten representative regions of interest (ROIs) measuring 50×50 pixels within each image were chosen manually for the analysis. A histogram for each ROI was calculated, and the fluorescence intensity was determined as the gray level corresponding to the histogram peak. The mean fluorescence intensity over the ten ROIs was calculated for each image and divided by 256 (2^8 intensity values) to provide the relative fluorescence intensity (RFI). The RFIs were further normalized to the RFI signal from free anti-*HER2* antibody, which represented the maximum binding. These normalized RFIs (NRFIs) provided quantification of the efficiency of treatment with Ab-Dex-MNPs or Dex-MNPs.

3. Results and Discussion

3.1. *Size determination of targeted magnetic nanoparticles by TEM*

TEM analysis revealed that the size of the Dex-MNP and Ab-Dex-MNP particles was approximately 20 to 30 nm (Fig. 1). The MNPs appear mostly monodispersed, with little to no aggregate formation. Particles in the range of 30 to 100 nm can usually avoid rapid leakage from the blood capillaries, whereas particles larger than 100 nm move more slowly and are more susceptible to clearance by interstitial macrophages. Larger particles (>200 nm) are more efficient at activating the complement system and they are cleared faster from the circulation by Kuppfer cells.[41] Hence, based on the size and coating characteristics of our MNPs, a longer circulation life span for *in vivo* studies is expected.

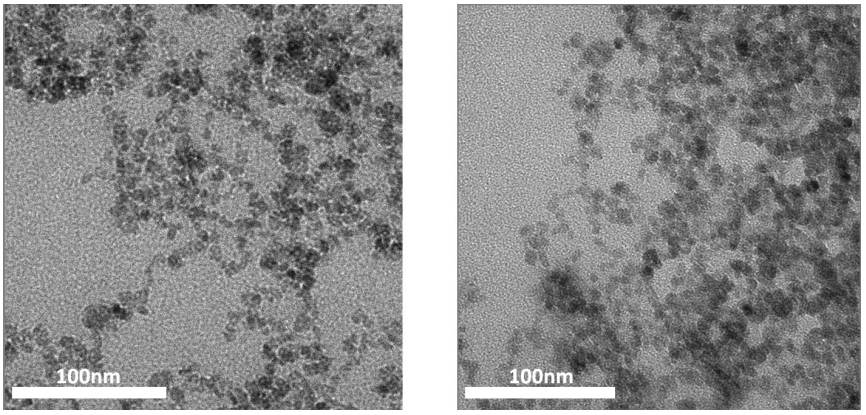

Fig. 1. TEM images of Ab-Dex-MNPs (left) and Dex-MNPs (right).

3.2. *Fc-directed method of conjugation*

A conjugation method to engineer efficient antibody-targeted nanoparticles should maximize the free and specific targeting active sites. There are many different sites on an antibody molecule, such as hydroxyl, carboxyl, amino, and sulfidryl or thiol groups, that can be used for this purpose. Among them, the conjugation methods which target primary amino groups by using the reagent carbodiimide hydrochloride (EDC) [N-ethyl-N-(3-dimethylaminopropyl)] are the least effective. In each monomeric antibody molecule such as IgG, only two primary and an abundant number of secondary amino groups are present. Hence, binding the primary amino groups to a nanoparticle will significantly reduce the antibody activity and the targeting sensitivity. To overcome this problem, we used an Fc-directed conjugation, to exclude the active sites from being involved in conjugation, hence keeping them intact for active and efficient targeting.

3.3. *Characteristics and advantages of our engineered MNPs*

A macrophage cell line, which is known to have multiple Fc receptors on the cell surface, was used to demonstrate that the antibody molecules were mostly bound through the Fc portion on the antigen and not through the active sites (Fig. 2).

Different cell lines were used to test the activity, specificity, and sensitivity of our engineered targeted MNPs using a solid phase indirect immunofluorescence assay. The results show that binding of the Ab-coated MNPs obtained by the Fc-directed conjugation method is significantly less (Fig. 3, middle) than binding observed with free

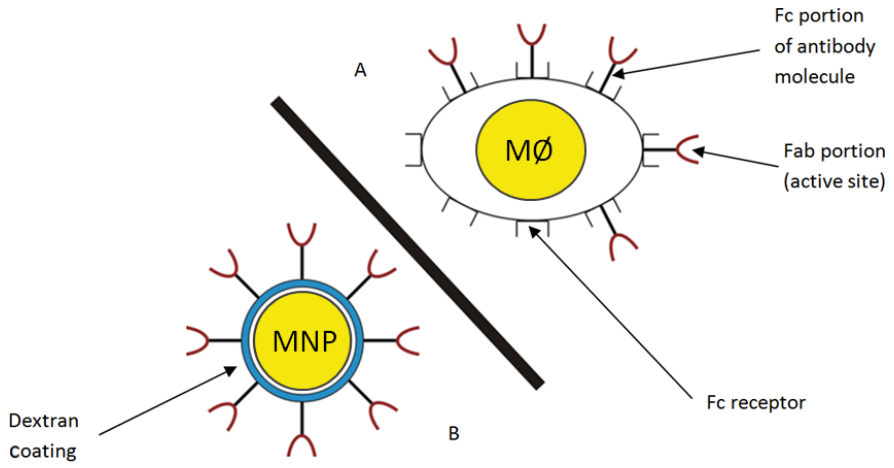

Fig. 2. Schematic representation of comparative binding capacities of free (A) and bound (B) antibody molecules to the surface of macrophages (MØ). Diagram (A) illustrates that free, unbound anti-*HER2* antibody can easily bind to the Fc receptors present on the surface of macrophages, while the binding of the Fc-directed MNPs, conjugated with the same antibody, will be greatly reduced or even completely blocked. The diagonal black line in the figure schematically represents the blockage of binding of targeted MNPs to the surface of macrophages through the Fc receptors.

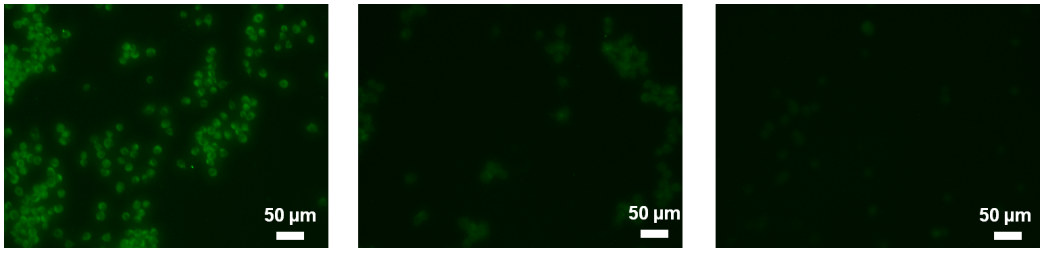

Fig. 3. Macrophages immunostained with free anti-*HER2* antibody (left), Ab-Dex-MNPs (middle), and Dex-MNPs (right). The fluorescence signal is significantly reduced in the middle image compared to the left image, which indicates reduction of MNP binding due to the Fc-directed conjugation of the antibodies to the MNPs. The right image confirms the absence of non-specific binding of MNPs to the macrophages.

anti-*HER2* antibody (Fig. 3, left). The antibody molecule after conjugation with MNPs through its Fc portion can no longer bind to the Fc receptors present on the surface of the macrophages. This will result in leaving most of the antibody active sites (Fab portion) free and available for active and sensitive targeting. The results of immunochemical analysis also showed that the Fc portion of commercial anti-*HER2* antibody can strongly bind to the Fc receptors on the surface of macrophages (Fig. 3, left), while the non-targeted MNPs showed little or no binding (Fig. 3, right), representing the positive and negative controls respectively.

Rapid clearance of targeted nanoparticles by macrophages through the opsonin property of the Fc portion of the antibody molecule is usually the other main challenge in designing and utilizing different targeted nanoparticles. Fabricating specific nanoparticles with little to no free Fc portion greatly diminishes the opsonin role of the antibody molecule used for targeting. With this Fc-directed method of conjugation, the opsonin activity of the antibody molecule is masked, and therefore will likely reduce the endocytosis of MNPs by macrophages, resulting in their longer expected circulation time. Moreover, dextran and antibody (hydrophilic coating) provide a longer circulation half life for the engineered MNPs and a low rate of clearance by the RES. Finally, as the engineered MNPs are anionic, less cytotoxic effects are expected.

3.4. *Cell line targeting*

To demonstrate that our engineered MNPs are capable of actively targeting *HER2* receptors, immunostaining of different cell lines with different *HER2* expression levels was performed. The results confirm that the engineered targeted MNPs are capable of activly targeting *HER2* expression (Fig. 4) and can also differentiate between cell lines with different *HER2* expression levels (Figs. 5 and 6).

After calibrating the Relative Fluorescence Intensity (RFI) to 100% obtained by treating SKBR-3 cells with commercial anti-*HER2* antibody, as shown in Fig. 6, the normalized RFI (NRFI) for SKBR-3 cells treated with Ab-coated MNPs would be greater than 300. The signal from SKBR-3 cells treated with commercial anti-*HER2* theoretically represents the ideal binding conditions. The higher RFI obtained by Ab-coated MNPs can be attributed to multiple bound antibody molecules on each MNP, which may amplify the fluorescence intensity obtained by the indirect immunofluorescence assay. We estimated this amplification factor (AF $\approx$ 3) by dividing the NRFI of SKBR-3 cells treated with Ab-MNPs by the NRFI obtained from SKBR-3 cells treated with commercial anti-*HER2* antibody. The AF suggests that in the conjugation process, on average, binding of three antibody molecules per MNP occurs.

If we calibrate the fluorescence signal obtained from the macrophages treated with commercial

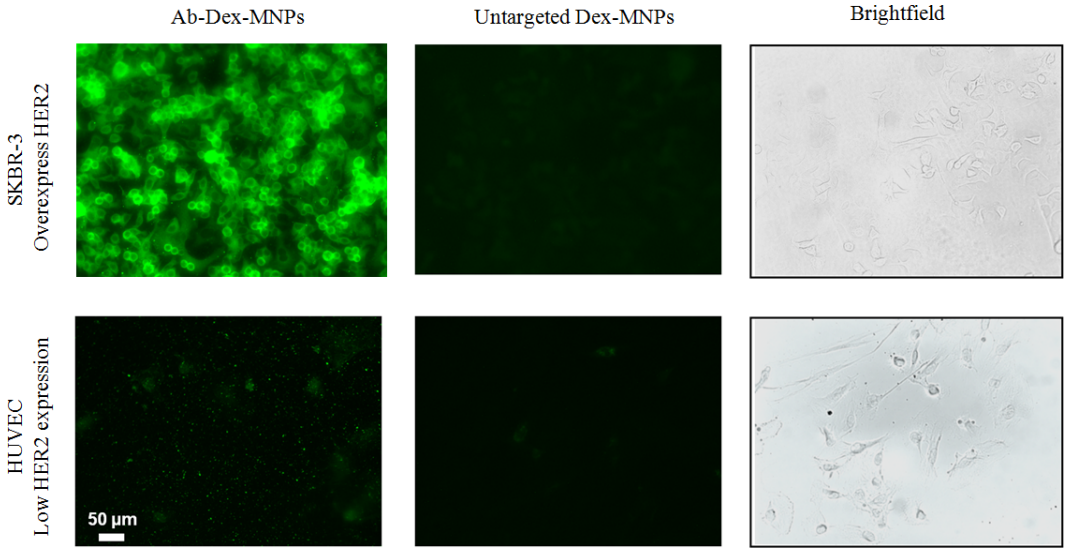

Fig. 4. Fluorescence microscopy of cells treated with Ab-Dex-MNPs (left column), untargeted Dex-MNPs (middle column), and brightfield images (right column). Two cell lines were tested: SKBR-3 cells, with overexpressed *HER2* (top row) and HUVEC cells with low *HER2* expression (bottom row).

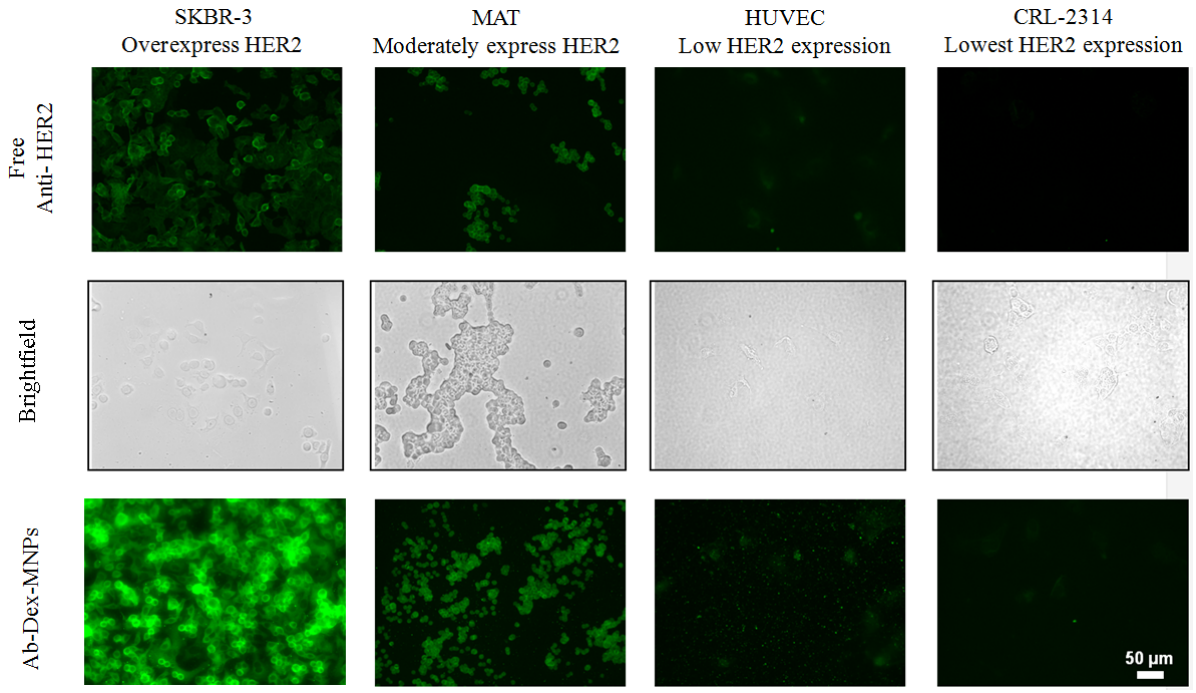

Fig. 5. Different cell lines immunostained using free anti-*HER2* (top row) and Ab-Dex-MNPs (bottom row). The cell lines are indicated above each column. The middle row shows the brightfield images of the different cell lines.

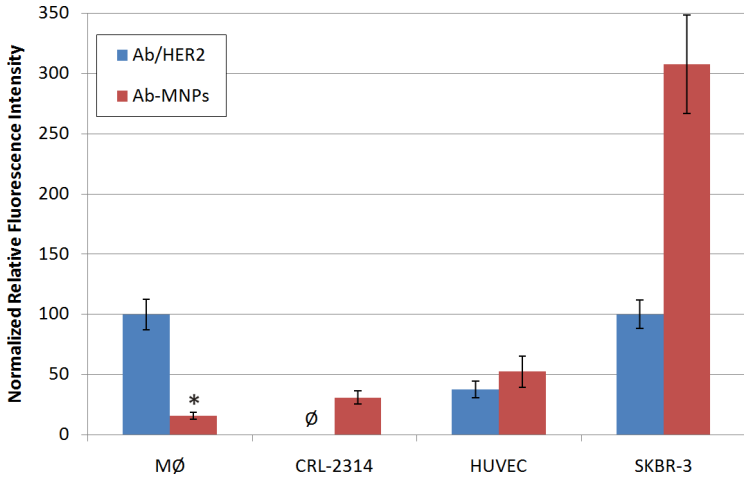

Fig. 6. Relative fluorescence intensity from different cell lines obtained using free anti-*HER2* antibody and targeted Ab-Dex-MNPs. Symbol Ø in the case of CRL-2314 cell line with minimal *HER2* expression, indicates that there was no fluorescence signal after exposure to free anti-*HER2* antibody. Macrophages (MØ) were used to detect the fraction of Fab-conjugated MNPs. For each cell line, the difference in RFI between Ab/HER2 and Ab-MNP binding is statistically significant ($p < 0.005$). *Value of normalized relative fluorescence intensity (NRFI) divided by amplification factor (AF).

anti-*HER2* antibody to 100%, then the NRFI for macrophages treated with Ab-MNPs is calculated to be 16%, after dividing by the AF. This means that if we assume that 100% of the commercial anti-*HER2* antibody have the Fc portion available to be bound to macrophage Fc receptors, only 16% of targeted MNPs may have any available terminal Fc sites for this kind of binding. Considering the fact that normal cells such as macrophages may express low levels of the *HER2* marker, we can conclude that even more than 84% of the antibody molecules were attached to the MNPs through their Fc portions.

In 2007, Grüttner, *et al.*, conjugated magnetic nanoparticles using different methods and

approaches.[31] In their well-designed two-step immunoassay, they calculated the highest percentage for a maleimide-based method to be ∼60% and for a carbodiimide-based method to be ∼20%. In their calculations, however, they did not consider the fact that the secondary anti-immunoglobulin not only can recognize the Fc portion of an antibody molecule attached to the MNP through its Fab portion, but also can fully recognize the multiple antigenic determinants present on the Fc portion of an antibody molecule, even if attached through the Fc portion. Therefore, the total measurements should potentially be at least half of the reported values. Using the carbodiimide-based method of conjugation as an example, which usually targets the primary amino group of the antibody molecule present on the Fab portion, the correct calculated percentage would likely be less than 10%. This means that at least 90% of the antibody molecules will likely be attached to the MNPs through their Fab portion or their active sites. Therefore, by following the carbodiimide-based method of conjugation, one may lose 90% of the antibody activity, leaving only 10% for active targeting. By following the Fc-directed conjugation described in this paper, over 84% of the active sites are likely to remain free for specific and sensitive targeting.

4. Conclusion

In this study, we have engineered superparamagnetic dextran-coated iron oxide nanoparticles to be used as specific anti-*HER2* antibody-targeted MNPs for active molecular targeting. In our selected way of conjugation, the Fc portion of the antibody molecule binds to the surface of the magnetic nanoparticle and the Fab portion (active site) of the antibody molecule remains intact and available for specific targeting, as was demonstrated on different cell lines with different levels of *HER2* expression.

Based on the size, negative charge, hydrophilic surface, dispersibility, and Fc-directed-conjugation, this molecular probe is a promising candidate for *in vivo* applications due to its longer predicted circulation lifetime and reduced clearance rate by macrophages. The probe can potentially be used to enhance contrast in imaging modalities such as MRI and magnetomotive optical coherence tomography. Finally, this molecular probe has the potential for targeted *in vivo* therapy using magnetically induced drug release or for site-specific hyperthermia treatments in cancer therapy.

Acknowledgments

We would like to thank Scott Robinson from the Imaging Technology Group at the Beckman Institute for Advanced Science and Technology for his assistance with TEM analysis. This research was supported in part by grants from the National Institutes of Health (Roadmap Initiative, NIBIB, R21 EB005321, S.A.B., and NIBIB, R01 EB005221, S.A.B.).

References

1. E. E. Graves, R. Weissleder, V. Ntziachristos, "Fluorescence molecular imaging of small animal tumor model," *Current Molecular Medicine* **4**, 419–430 (2004).
2. D. R. Larson, W. R. Zipfel, R. M. Williams, S. W. Clark, M. P. Bruchez, F. W. Wise, W. W. Webb, "Water-soluble quantum dots for multiphoton fluorescence imaging *in vivo*," *Science* **300**, 1434–1436 (2003).
3. X. H. Gao, Y. Y. Cui, R. M. Levenson, L. W. K. Chung, S. M. Nie, "*In vivo* cancer targeting and imaging with semiconductor quantum dots," *Nat. Biotechnol.* **22**, 969–976 (2004).
4. S. Kim, Y. Y. Lim, E. G. Soltesz, A. M. D. Grand, J. Lee, A. Nakayama, J. A. Parker, T. Mihaljevic, R. Laurence, L. H. Cohn, M. G. Bawendi, J. V. Frangioni, "Near-infrared fluorescent type II quantum dots for sentinel lymph node mapping," *Nat. Biotechnol.* **22**, 93–97 (2004).
5. J. Czernin, M. E. Phelps, "Positron emission tomography scanning: Current and future applications," *Ann. Rev. Med.* **53**, 89–112 (2002).
6. G. D. Luker, D. Piwnica-Worms, "Molecular imaging *in vivo* with PET and SPECT," *Acad. Radiol.* **8**, 4–14 (2001).
7. P. A. Dayton, D. Pearson, J. Clark, S. Simon, P. A. Schumann, R. Zutshi, T. O. Matsunaga, K. W. Ferrara, "Ultrasonic analysis of peptide- and antibody-targeted microbubble contrast agents for molecular imaging of $\alpha v\beta 3$-expressing cells," *Molecular Imaging* **3**, 125–134 (2004).
8. J.-H. Lee, Y.-M. Huh, Y.-W. Jun, J.-W. Seo, J.-T. Jang, H.-T. Song, S. Kim, E.-J. Cho, H.-G. Yoon, J.-S. Suh, J. Cheon, "Artificially engineered magnetic nanoparticles for ultra-sensitive molecular imaging," *Nat. Med.* **13**, 95–99 (2007).
9. M. A. Funovics, B. Kapeller, C. Hoeller, H. S. Su, R. Kunstfeld, S. Puig, K. Macfelda, "MR imaging of the HER2/neu and 9.2.27 tumor antigens using immunospecific contrast agents," *Magn. Reson. Imaging* **22**, 843–850 (2004).
10. I. H. El-Sayed, X. H. Huang, M. A. El-Sayed, "Surface plasmon resonance scattering and absorption of

anti-EGFR antibody conjugated gold nanoparticles in cancer diagnostics: Applications in oral cancer," *Nano Lett.* **5**, 829–834 (2005).
11. S. A. Boppart, A. L. Oldenburg, C. Xu, D. L. Marks, "Optical probes and techniques for molecular contrast enhancement in coherence imaging," *J. Biomed. Opt.* **10**, 1–14 (2005).
12. T. M. Lee, F. J. Toublan, S. Sitafalwalla, A. L. Oldenburg, K. S. Suslickm, S. A. Boppart, "Engineered microsphere contrast agents for optical coherence tomography," *Opt. Lett.* **28**, 1546–1548 (2003).
13. A. L. Oldenburg, F. J. Toublan, K. S. Suslick, A. Wei, S. A. Boppart, "Magnetomotive contrast for *in vivo* optical coherence tomography," *Opt. Exp.* **13**, 6597–6614 (2005).
14. C. Loo, A. Lowery, N. Halas, J. West, R. Drezek, "Immunotargeted nanoshells for integrated cancer imaging and therapy," *Nano Lett.* **5**, 709–711 (2005).
15. N. Desai, V. Trieu, Z. W. Yao, L. Louie, S. Ci, A. Yang, C. Tao, T. De, B. Beals, D. Dykes, P. Noker, R. Yao, E. Labao, M. Hawkins, P. Soon-Shiong, "Increased antitumor activity, intratumor paclitaxel concentrations, and endothelial cell transport of cremophor-free, albumin-bound paclitaxel, ABI-007, compared with cremophor-based paclitaxel," *Clin. Cancer Res.* **12**, 1317–1324 (2006).
16. R. Weissleder, A. Bogdanov, E. A. Neuwelt, M. Papisov, "Long-circulating iron oxides for MR imaging," *Adv. Drug Delivery Rev.* **16**, 321–334 (1995).
17. J. Sinek, H. Frieboes, X. Zheng, V. Cristini, "Two-dimensional chemotherapy simulations demonstrate fundamental transport and tumor response limitations involving nanoparticles," *Biomedical Microdevices* **6**, 297–309 (2004).
18. B. Schade, S. H. L. Lam, D. Cernea, V. Sanguin-Gendreau, R. D. Cardiff, B. L. Jung, M. Hallett, W. J. Muller, "Distinct ErbB-2–coupled signaling pathways promote mammary tumors with unique pathologic and transcriptional profiles," *Cancer Res.* **67**, 7579–7589 (2007).
19. N. W. Shi Kam, M. O'Connell, J. A. Wisdom, H. Dai, "Carbon nanotubes as multifunctional biological transporters and near-infrared agents for selective cancer cell destruction," *Proc. Natl. Acad. Sci. U.S.A.* **102**, 11600–11605 (2005).
20. S. J. DeNardo, G. L. DeNardo, L. A. Miers, A. Natarajan, A. R. Foreman, C. Grüettner, G. N. Adamson, R. Ivkov, "Development of tumor targeting bioprobes (in-chimeric L6 monoclonal antibody nanoparticles) for alternating magnetic field cancer therapy," *Clin. Cancer Res.* **11**, 7087–7092 (2005).
21. P. Sharma, S. C. Brown, G. Walter, S. Santra, E. Scott, H. Ichikawa, Y. Fukumori, "Gd-nanoparticulates: From magnetic resonance imaging to neutron capture therapy," *Adv. Powder Techn.* **18**, 663–698 (2007).
22. N. Nasongkla, E. Bey, J. Ren, H. Ai, C. Khemtong, J. S. Guthi, S.-F. Chin, A. D. Sherry, D. A. Boothman, J. Gao, "Multifunctional polymeric micelles as cancer-targeted, MRI-ultrasensitive drug delivery systems," *Nano Lett.* **6**, 2427–2430 (2006).
23. X.-H. Peng, X. Qian X, H. Mao, A. Y. Wang, Z. Chen, S. Nie, D. M. Shin, "Targeted magnetic iron oxide nanoparticles for tumor imaging and therapy," *Intl. J. Nanomedicine* **3**, 311–321 (2008).
24. Y. X. J. Wang, S. M. Hussain, G. P. Krestin, "Superparamagnetic iron oxide contrast agents: Physicochemical characteristics and applications in MR imaging," *European Radiology* **11**, 2319–2331 (2001).
25. C. C. Berry, S. Wells, S. Charles, G. Aitchison, A. S. G. Curtis, "Cell response to dextran-derivatised iron oxide nanoparticles post internalization," *Biomaterials* **25**, 5405–5413 (2004).
26. H. Lee, E. Lee, D. K. Kim, N. K. Jang, Y. Y. Jeong, S. Jon, "Antibiofouling polymer-coated superparamagnetic iron oxide nanoparticles as potential magnetic resonance contrast agents for *in vivo* cancer imaging," *J. Am. Chem. Soc.* **128**, 7383–7389 (2006).
27. A. K. Gupta, M. Gupta, "Synthesis and surface engineering of iron oxide nanoparticles for biomedical applications," *Biomaterials* **26**, 3995–4021 (2005).
28. J. R. McCarthy, R. Weissleder, "Multifunctional magnetic nanoparticles for targeted imaging and therapy," *Adv. Drug Delivery Rev.* **60**, 1241–1251 (2008).
29. D. Simberg, T. Duza, J. H. Park, M. Essler, J. Pilch, L. Zhang, A. M. Derfus, M. Yang, R. M. Hoffman, S. Bhatia, M. J. Sailor, E. Ruoslahti, "Biomimetic amplification of nanoparticle homing to tumors," *Proc. Nat. Acad. Sci. U.S.A.* **104**, 932–936 (2007).
30. F. Ibraimi, D. Kriz, M. Lu, L.-O. Hansson, K. Kriz, "Rapid one-step whole blood C-reactive protein magnetic permeability immunoassay with monoclonal antibody conjugated nanoparticles as superparamagnetic labels and enhanced sedimentation," *Analytical and Bioanalytical Chem.* **384**, 651–657 (2006).
31. C. Grüttner, K. Müller, J. Teller, F. Westphal, A. Foreman, R. Ivkov, "Synthesis and antibody conjugation of magnetic nanoparticles with improved specific power absorption rates for alternating magnetic field cancer therapy," *J. Magnetism and Magnetic Materials* **311**, 181–186 (2007).
32. E. Okon, D. Pouliquen, P. Okon, Z. V. Kovaleva, T. P. Stepanova, S. G. Lavit, B. N. Kudryavtsev, P. Jallet, "Biodegradation of magnetite dextran nanoparticles in the rat: A histologic and biophysical study," *Laboratory Investigation* **71**, 895–903 (1994).

33. H. Pardoe, W. Chua-Anusorn, T. G. St. Pierre, J. Dobson, "Detection limits for ferrimagnetic particle concentrations using magnetic resonance imaging based on proton transverse relaxation rate measurements," *Physics in Medicine and Biology* **48**, N89–N95 (2003).
34. J. W. Park, K. Hong, D. B. Kirpotin, G. Colbern, R. Shalaby, J. Baselga, Y. Shao, U. B. Nielsen, J. D. Marks, D. Moore, D. Papahadjopoulos, C. C. Benz, "Anti-HER2 immunoliposomes enhanced efficacy attributable to targeted delivery," *Clin. Cancer Res.* **8**, 1172–1181 (2002).
35. J. M. Perez, F. J. Simeone, Y. Saeki, L. Josephson, R. Weissleder, "Viral-induced self-assembly of magnetic nanoparticles allows the detection of viral particles in biological media," *J. Am. Chem. Soc.* **125**, 10192–10193 (2003).
36. H. Tada, H. Higuchi, T. M. Wanatabe, N. Ohuchi, "*In vivo* real-time tracking of single quantum dots conjugated with monoclonal anti-HER2 antibody in tumors of mice," *Cancer Res.* **67**, 1138–1144 (2007).
37. M. B. Wilson, P. K. Nakane, "The covalent coupling of proteins to periodate-oxidized sephadex: A new approach to immunoadsorbent preparation," *J. Immunol. Methods* **12**, 171–181 (1976).
38. J. M. C. Luk, A. A. Lindberg, "Rapid and sensitive detection of Salmonella (O: 6,7) by immunomagnetic monoclonal antibody-based assays," *J. Immunol. Methods* **137**, 1–8 (1991).
39. L. X. Tiefenauer, G. Kühne, R. Y. Andres, "Antibody-magnetite nanoparticles: *In vitro* characterization of a potential tumor-specific contrast agent for magnetic resonance imaging," *Bioconjugate Chem.* **4**, 347–352 (1993).
40. F. Bonneaux, E. Dellacherie, P. Labrude, C. Vigneron, "Hemoglobin-dialdehyde dextran conjugates: Improvement of their oxygen-binding properties with anionic groups," *J. Protein Chem.* **15**, 461–465 (1996).
41. S. M. Moghimi, A. C. Hunter, J. C. Murray, "Nanomedicine: Current status and future prospects," *FASEB J.* **19**, 311–330 (2005).